Hydrogenated-Graphene encapsulated Graphene: A versatile material for device applications

Mohammed Ghadiyali* and Sajeev Chacko**

Department of Physics, University of Mumbai, Kalina Campus, Santacruz (E), Mumbai - 400 098, India.

E-mail: ghadiyali.mohd@physics.mu.ac.in;
sajeev.chacko@physics.mu.ac.in;sajeev.chacko@gmail.com

Abstract

Graphene and its heterostructures exhibit interesting electronic properties and are explored for quantum spin Hall effect(QSHE) and magnetism based device-applications. In present work, we propose a heterostructure of graphene encapsulated by hydrogenated-graphene which could be a promising candidate for a variety of device applications. We have carried out DFT calculations on this system to check its feasibility to be a versatile material. We found that electronic states of multilayer pristine graphene, especially Dirac cone, an important feature to host QSHE, can be preserved by sandwiching it by fully hydrogenated-graphene. Interference of electronic states of hydrogenated-graphene was insignificant with those of graphene. States of graphene were also found to be stable upon application of electric field up-to 2.5V/nm. For device applications, multilayer-graphene or its heterostructures are required to be deposited on a substrate, which interacts with system opening up a gap at Dirac cone making it less suitable for QSHE applications and hydrogenated-graphene can prevent it. Magnetization in these

1

hydrogenated-graphene sandwiched graphene may be induced by creating vacancies or distortions in hydrogenated-graphene, which was found to have minimal effect on grapheneâ ĂŹs electronic states, thus providing an additional degree of manipulation. We also performed a set of calculations to explore its applicability for detecting some molecules. Our results on trilayer-graphene encapsulated by hydrogenated-graphene indicate that all these observations can be generalized to systems with a larger number of graphene layers, indicating that multilayer-graphene sandwiched between two hydrogenated-graphene is a versatile material that can be used in QSHE, sensor devices, etc.

Introduction

The honeycomb lattice structure of graphene (GR) is the nearest analogy to Haldaneâ ĂŹs model[1] in condensed matter physics. However, due to the weak spin-orbital coupling (SOC) of carbon atoms, it is not an ideal quantum spin Hall insulator (QSHI) or 2D topological insulator.[2] Quantum spin Hall effect (QSHE) is realized in GR, but the band gap of GR is zero, limiting its application. For this reason, a lot of work has been devoted to finding an alternative QSHI with high SOC and high bulk band gap. A non-Haldaneâ ĂŹsmodel system HgTe quantum well has been found to be a good alternative. However, it requires low operating temperature which hinders its applications.[3] Further, 2D allotropes of group VI(A) and V(A) have also been predicted to be QSHI.[4] Out of these, stanene (a 2D allotrope of tin) has been reported to meet most of the requirements and has been studied both theoretically and experimentally.[5–8]

Even after all these developments, GR, both in pristine as well as heterostructures forms are still being investigated for QSHE.[9,10] To preserve the QSHI nature, GR is generally coupled with 2D boron-nitrate (2D-BN) as a heterostructure, fabricated by alternating layers of GR and 2D BN.[11] Apart from 2D BN, other 2D materials like WS_2[12] and MoS_2[13] - inducing spin-orbital coupling, yttrium iron garnet,[14,15] and EuS[16] - inducing ferromagnetism,

MoSe$_2$[17] - fabrication of Schottky devices, etc, have been studied for various applications. One of the biggest drawbacks of these heterostructures is they strain GR, opening up a band gap in the place of Dirac cone and fabrication of these above-mentioned structures is not a trivial process, as explained further in the text. In the present work, we propose an alternative to this system by replacing the 2D BN with hydrogenated-GR (HG). This substitution preserves the essential Dirac cone of the GR layer enabling the composite multilayer system to host QSHE. However, there are certain benefits to this approach over the GR-BN heterostructures as discussed below.

Mismatch in the lattices between the graphene and other layers may have profound effects on its structural and electronic properties. For instance, a moirÃľ pattern is seen in the crystal structure of the GR-BN heterostructures as a consequence of slight mismatch of their lattice vectors.[18] However, these are reported to form inside the GR and their effects on the QSHI states is required to be studied in detail. Such an effect breaks the inversion symmetry of the GR opening up a band gap. Further, the QSHI states in GR are reported to be quite fragile due to which high quality and a defect-free sample is required. The preferred method has been to mechanically exfoliate the sheets of GR via scotch tape process.[19,20] This process is also repeated for the fabrication of 2D BN sheets and then these sheets are stacked on each other in the required orientation. Though this yields a high purity and defect-free sample, it requires a high level of skill and is time-consuming. While a method like chemical vapor deposition is used, it creates nanoflakes of GR rather than a continuous film.[21] Other than that strain matching GR and 2D BN is again a complex process.[22,23] Hence, the large-scale extension of this process is challenging.

On the other hand, to fabricate the proposed systems one needs to exfoliate multilayer graphene and only hydrogenate the outermost layer. A similar technique has been implemented for the fabrication of heterostructure of GR and monolayer transition-metal dichalcogenides.[24] Or the recent developments in the fabrication of high-quality graphene can be used for the same.[25] In addition, the magnetization in HG can be modulated via photolithographic

3

processes.[26] Such modulations in the proposed GR-HG heterostructures can be used to tune its properties for desired magnetic applications. We demonstrate this tunability for GR and HG trilayer nanoribbons. Hence, the present work is divided into two parts: In the first part, we discuss the stability of the proposed systems and the role of HG in preserving the essential electronic states of the GR layer. As the dimensions of the gate in nanodevices is being reduced, it can be described as 1D structures. Hence, in the second part, we construct nanoribbons of up to 20 unit cells [1] to study magnetization in it. We also explore the ability of the HG-GR trilayer to adsorb simple molecules such as H_2, O_2, CO_2, and ethanol.

Computational Details

We have performed the first principle density functional theory (DFT) calculations as implemented in the Quantum ESPRESSO (QE)[28] package. We have used Perdew-Burke-Ernzerhof (PBE)[29] exchange-correlation function and included the DFT-D2 van der Waals corrections[30,31] for representing the electron dispersion effect induced due to the multi-layer nature of the systems. A Γ-centered Monkhorst-pack k-point grid of $15 \times 15 \times 1$ gave was sufficient to sample the irreducible Brillouin zone. A kinetic energy cutoff of 40 Ry for the wavefunctions gave the required convergence in the total energy. This energy cutoff has been used in all the calculations presented in this work. The pseudopotentials used in this work were obtained from the PSlibrary version 1.0.[32,33] Further, to limit the interaction between the periodic images of the unit cell, a vacuum of ≈ 10Åis added to the unit cell above and below the trilayer system. The geometry optimization was performed until the forces per atom were reduced to less than 10^{-6} Ha/au. The phonon spectra calculations of the systems were performed by the density-functional perturbation method, as implemented in QE.

To compute the edge states, nanoribbons were constructed having a width of up to 20 unit cells along the y-direction and a single unit cell in the X-direction. To minimize the

---

[1]With the available computational facility we could do the calculations only for a maximum of 20 unit cells. However, in order to observe QSHE a much wider nanoribbon of up to about 50 unit cells may be required[27]

interactions from neighboring images, a vacuum of $\approx 10\text{Å}$ was added on both sides along Y and Z-directions. The k-point mesh of $6 \times 1 \times 1$ was used. A small and arbitrary initial value of the magnetic moment was set for each atom for the spin-polarized calculations and a full geometry optimization was carry out to obtain the final magnetic state. For computing the band structures, high symmetry k-points of the Brillouin zone were selected along the path $M \to \Gamma \to K \to M$. The k-points were generated by the XCrysDens package.[34] It may be noted that we have not considered spin-orbit coupling since as it is quite weak in carbon and hydrogen atoms.

We studied two types of trilayer systems: (1) single GR layer sandwiched between two HG layers denoted as system A and (2) single HG layer sandwiched between two GR layers denoted as system B as illustrated in figures 1(c)and 1(d), respectively. As these are multilayer systems, the stacking angle is also an important feature. The two selected different stacking angles are 0°generally noted as AB configuration and 60°generally denoted as AA configuration, as shown in figures 1(a) and 1(b), respectively. The selection of the stacking angle was done in accordance with the Bernal stacking method. For convenience, the systems have been named using the following nomenclature: a prefix is used to denote trilayer configuration and postfix to indicate the stacking angle.

As an example, the system of GR encapsulated by HG with stacking angle of 0°is named as "A0", while the system where HG is encapsulated by GR with stacking angle of 60°is named as "B60". Hence the structures have been named as A0, A60, B0, and B60. Similar configurations for the bilayer systems were also studied. However, from the phonon dispersion calculations, they were found to be very unstable and hence not considered for the presented work. The crystal and band structure details regarding these additional systems can be found in the SI section VI. The systems described in the text had been generated using ATK Virtual Nano Lab.[35]
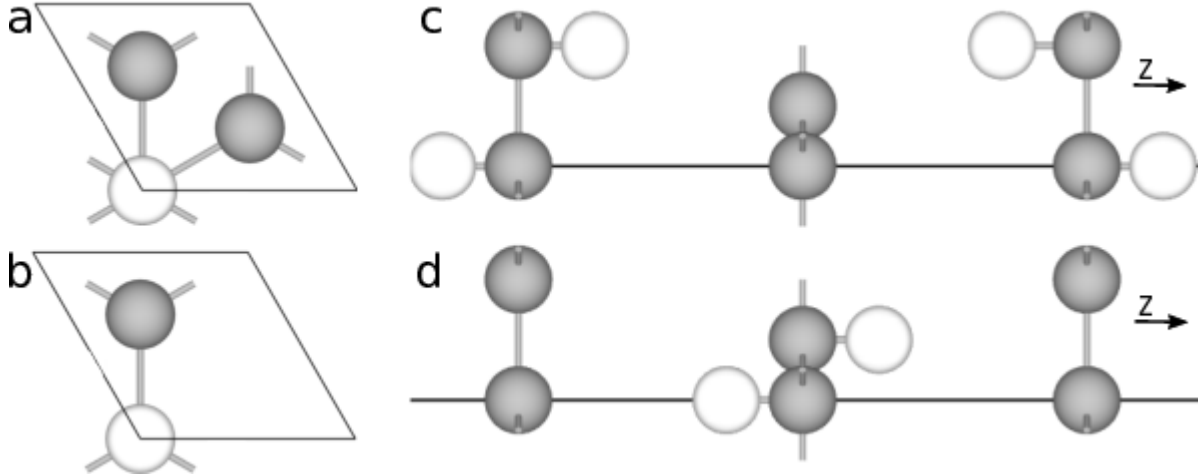
Figure 1: Configuration of trilayer HG-GR systems. (a) and (b) Top view the two different stacking angles (0°and 60°, respectively), The axis of rotation is the z-axis that is perpendicular to the plane of the paper. (c) and (d) Different stacking orders (HG-GR-HG and GR-HG-GR, respectively). These structures are before geometry optimization.

Results and Discussion

QSHE in Graphene - HG heterostructures

We first discuss the structures of the the GR-HG heterosystems and their stability. We then describe by their band structures followed by the effect of electric field on the electronic structure properties of these heterostructures.

Structure and Stability of Proposed Systems

In figure 2, we display the optimized structures as well as phonons dispersion for A0, A60, B0 and B60 systems. The carbon atoms present in the plane of the HG layers is buckled due to the bonding with hydrogen atoms. A slight lateral displacement of the outer layers is also seen with respect to the central layer for A0 and B0 systems. The layers however approximately retain their stacking angles with respect to the central plane. Such a behavior has been reported in the 3R-type MoS_2 system[36] where one of the layers when laterally moved in the plane, showed a second energy minimum. The optimized lattice constant of A-type

and B0 and B60 was found to be 2.50, 2.50, 2.48 and 2.48 ÃĚ, respectively. Note that the lattice constant for graphene is 2.46 ÃĚ. Thus, the lattice mismatch between our proposed systems and pristine graphene is less than 1.5%, it is important merit for the proposed systems.
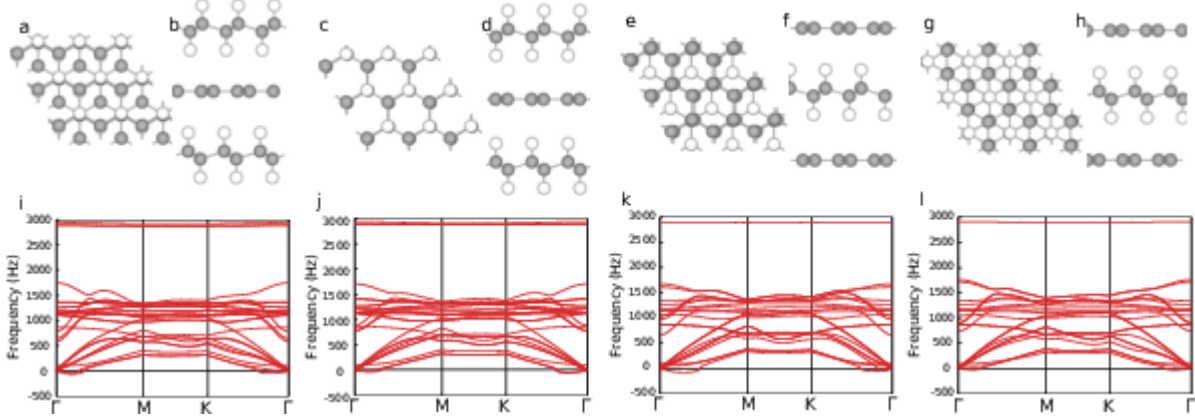

Figure 2: (color online) (a) Top and (b) side views of A0 system, (c) top and (d) side view of A60 system, (i), (j) phonon dispersion of the systems A0 and A60, respectively, plotted along the high-symmetry k-path, (e) Top and (f) side views of B0 system, (g) top and (h) side view of B60 system (i), (j) phonon dispersion of the systems B0 and B60, respectively, plotted along the high-symmetry k-path.

To understand the stability of the systems, phonon dispersion were calculated (figure 2. Most of the phonon frequencies are positive with a few exceptions primarily in the vicinity of Γ-point for most of the systems. The spread along the k-axis of these negative frequencies is also small and likely to be due to numerical errors rather than the instability in structure (See reference[37] for further explanation). The stability of these systems can further be checked based on its cohesive and formation energies. The energy of formation of trilayer from monolayers and the binding energy per atom can be calculated as:

$$
\begin{aligned}
E_{\text{formation}} &= E_{\text{trilayer}} - \sum E_{\text{layers}} \\
E_{\text{cohesive}} &= \frac{E_{\text{trilayer}} - \sum E_{\text{atom}}}{N_{\text{atoms}}}
\end{aligned}
$$

Negative values of these energies suggest that the system is thermodynamically stable i.e. the processes which can decompose and(or) transform these systems are either forbidden and(or) very gradual. In table 1, we show the energy of formation of trilayer from monolayers and the binding/cohesive energy per atom. Taking into account the magnitude of the values from the last column of the table, it may be concluded that the systems are energetically and thermodynamically favorable.

The negative frequencies near the Γ point do not necessarily mean the system is unstable as in this case the energetics are favorable. This has been demonstrated in the work of Mounet et al.,[38] where a screening of 2D materials from 3D bulk was performed with the help of high throughput methodology. This lead to the creation of a database of 2D materials which includes crystal structure, electronic band structure, and phonon dispersion. They have classified the materials with negative frequencies near the gamma point as stable as their energetics were favorable. Further, as the hydrogenated graphene layer is under strain it will give rise to negative frequencies and as mentioned above, it does not imply that the system is unstable. With these arguments, we may conclude that the systems under consideration are stable.

Table 1: The formation and binding energies of the trilayer systems.

Name	Total Energy (Ry)	Energy of trilayer formation (Ry)	Binding/Cohesive Energy per atom (Ry)
Graphene	-36.8942	-	-0.6805
Hydrogenated Graphene	-39.2646	-	-0.4737
A0	-115.4449	-0.0214	-0.5172
A60	-115.4429	-0.0194	-0.5170
B0	-113.0683	-0.0153	-0.5790
B60	-113.0694	-0.0163	-0.5792
Energy of isolated carbon atom		-17.7666 Ry	
Energy of isolated hydrogen atom		-0.9183 Ry	

Electronic Band structure of Proposed Systems

The band structures for all the systems were calculated to assert the feasibility of proposed systems to host QSHE. In figure 3, we show the band structures for all the configurations. Clearly, from the plot, we can note that for the different configurations of the proposed systems, the stacking order or stacking angles seems have little to no effect on the band structure of the sandwiched layer. The band structures of all systems were found to be quite similar, as they consist of the same components arranged in different configurations. From the initial observation, it may be noted that at the K-point there is a Dirac point similar to that of pristine GR. However, there is a extremely small and negligible gap, which is less than the error of DFT calculations, hence it can be considered as gapless. There are also some additional bands flanking the Dirac point. These bands touch the Fermi level, effectively interacting with the Dirac point providing an indirect conduction path, indicating these systems to be semimetallic in nature. If the proposed systems are semimetallic then the possibility of them hosting QSHE is reduced. However, detailed analyses of the band structures show that they still hold a possibility of hosting QSHE.

For understanding these features further, we plot the k-resolved projected density of states (PDOS) given in supplementary information (SI) section V. From these plots, one can observe that the Dirac cone at the K-point is formed out of the carbon atoms of the GR sheet, with negligible contribution from the HG atoms. Further, the band structures of the individual pristine GR and HG do not interfere with each other indicating a weak chemical coupling between GR and HG. Hydrogen bonding is observed when the distance of the hydrogen with the heavier and high electronegative elements such as O, N, is of the order of 1.5-2.5 Å. However, the hydrogen atoms nearest to any of the carbon atoms from the GR layer is about 2.8 Åindicating negligible interaction between the HG and GR layers. In addition, the electron density overlap between these layers is also not present (see SI section IV). Thus, we may be concluded that the presence of the additional band does not affect or alter the presence of the Dirac cone and the origin of the Dirac cone in the system can be

9

attributed to the central GR plane, providing a possibility of hosting QSHI state.

In order to examine whether if the HG layer shields multilayer graphene, we studied trilayer graphene encapsulated by HG. Note that even in pristine trilayer graphene the Dirac cone is preserved and has a possibility of hosting QSHI states.[39] We compute the band structure of this system and found that the characteristics of trilayer graphene have been preserved (SI section II) supporting the above-mentioned claim. Thus, the electronic properties of the graphene layers seem to be protected by the HG layer. Recall, that for device applications, the multilayer graphene, which holds QSHE, is generally required to be deposited on a substrate. The substrate states then interact with the graphene system opening up a gap at the Dirac cone making it less suitable for QSHE related applications. One way to protect the graphene states would be to add an HG monolayer between the graphene and the substrate. However, we found that the HG-graphene bilayer itself is very unstable. Hence, it could be difficult to synthesize and then deposit on a substrate. On the other hand, our calculations on HG encapsulated monolayer, as well as trilayer graphene, indicate that upon deposition on a substrate the graphene states are likely to be protected by the HG layers thus retaining the property of graphene layers to host QSHE.
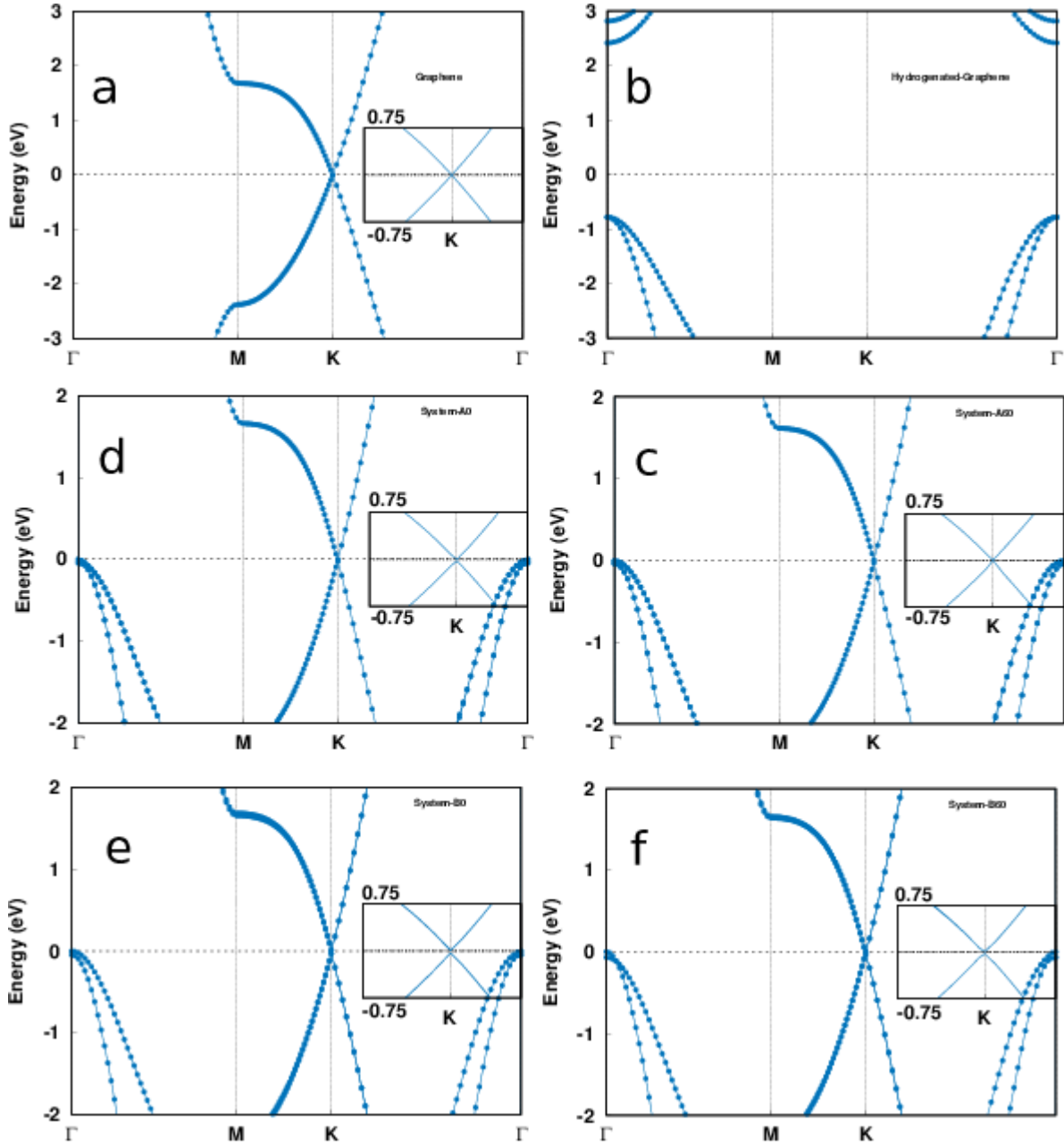
Figure 3: (color online) Band structures of (a) pristine graphene and (b) hydrogenated graphene. Band structures of the systems (c) A0, (d) A60, (e) B0, and (f) B60. Note that the Dirac point is present for the systems A0, A60, B0 and B60 (see inserts) and the band structure of the trilayer systems is basically an addition of the band structures of graphene and the HG band structure.

11

Effect of Electric Field on Band Structure of Proposed Systems

It is well known that the electronic structure of graphene is not affected due to the applied electric field. Hence, an application of an electric field to the HG-GR-HG trilayer should not affect the Dirac cone. In the buckled structure of 2D system such as silicene in the presence of the electric field, the potential felt by the sublattice is different which leads to an opening up of a band gap. Hence, in the presence of the electric field, if the HG layers due to its buckled nature interact with the graphene layer in the presence of an electric field, the Dirac cone may get altered. In order to probe the stability of Dirac cone in presence of the electric field, the HG-GR-HG trilayer systems in the A0 and A60 configurations were subjected to electric fields in the range from 0.0 to 2.5 V/nm in steps of 0.5 V/nm (see figure 4). The electric field is modeled by a saw-tooth potential which is purely a mathematical technique. Hence, care must be taken to set the boundary conditions so that the electric field drops to zero in the vacuum region away from the HG layers.
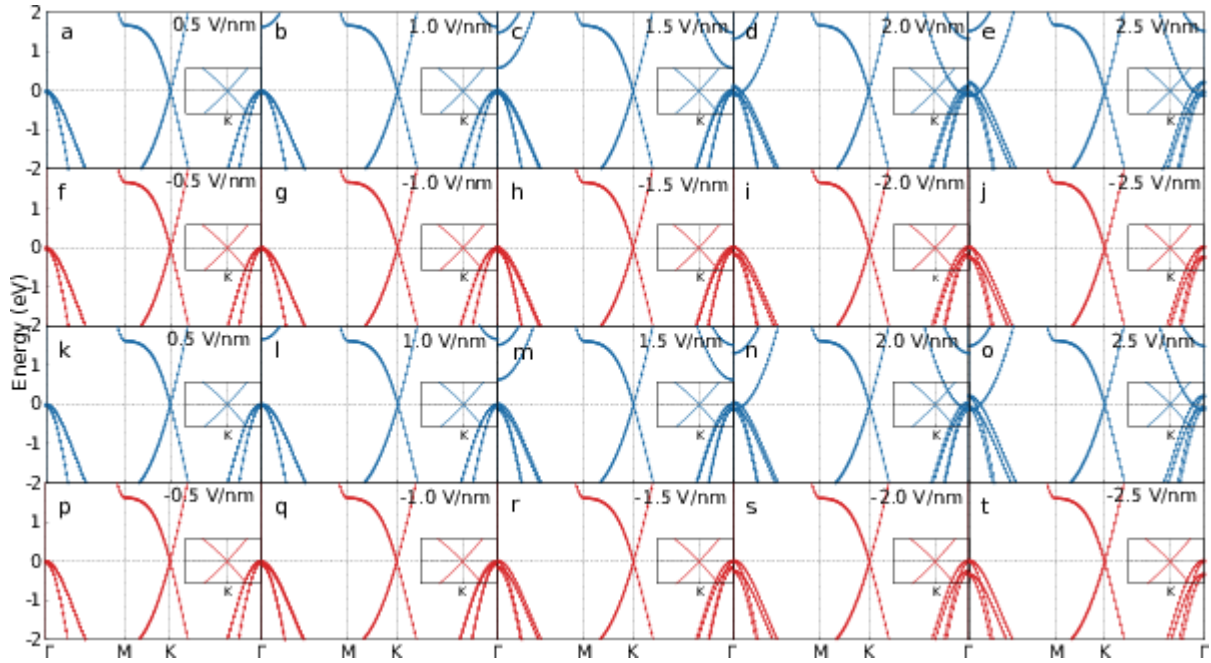

Figure 4: (color online) Band structures of system A0 (figures (a) to (j)) and A60 (figures (k) to (t)) under electric fields of 0.5, 1.0, 1.5, 2.0 and 2.5 V/nm. The energy range in the insert is form 0.75 eV to -0.75 eV.

Upon switching the electric field, we noted that the Dirac point present at the K-point is not affected at any given value of the electric field. A few bands in the vicinity of the Γ-point above and below the Fermi level do split. The projected density of states (PDOS) analyses shows that these bands are from the HG layer indicating that the HG states in A0 and A60 configurations do not interfere with the those of GR even in the presence of an electric field. Rather, it acts as a shield for the central GR layer. A similar conclusion can be made for the systems B0 and B60 (see figure 5). Unlike the A0 and A60 systems, here the Dirac point observed due to the GR sheets, is split albeit at high electric fields of about 4 V/nm and higher. Further, from figure 2, it can be observed that the range of negative phonon dispersion is higher when compared to the A0 and A60. Thus, one may conclude that in the A0 and A60 systems the Dirac point is quite stable. Hence, only these systems were considered for further investigation. From the above observations of the systems A0 and A60 and the derived conclusion, it is clear that the effect on the electronic states of GR is not unfavorably affected. Thus, the HG encapsulated GR holds a possibility of hosting QSHE.
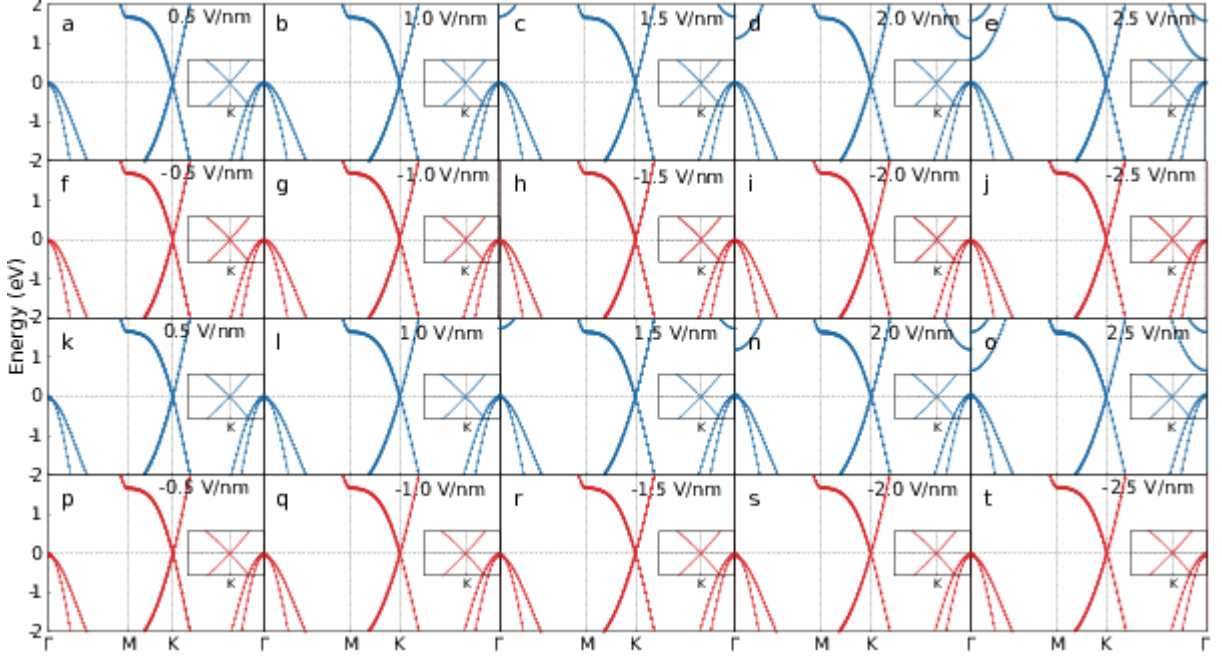
Figure 5: (color online) Band structures of system B0 (figures (a) to (j)) and B60 (figures (k) to (t)) under electric fields of 0.5, 1.0, 1.5, 2.0 and 2.5 V/nm. The energy range in the insert is form 0.75 eV to -0.75 eV.

A direct method of testing this claim would be calculating the Z_2 topological invariant where Z_2=1 means that the system is QSHI and Z_2=0 means the system is not QSHI. However, as these systems are constructed via stacking of multiple layers and the system as a whole is conducting, the current methods for determining the Z_2 invariant cannot be reliably used here.[2,40] An indirect method of determining if a system can host QSHE is to compute the edge state and to count the number of band crossings which should be odd numbered.[41] Even this method is difficult to implement since the systems A0 and A60 as a whole have an indirect band closing between the bands of GR (at the K-point above the Fermi level) and HG bands (near the Γ-point below the Fermi level) which will give the systems conducting edges. Thus, the only possible *ab-initio* method of determining whether the systems A0 and A60 can host the QSHE is to verify that the electronic states of GR are not affected. This has been performed and is concluded that electronic states are indeed not affected. Hence, the proposed systems A0 and A60 do have a possibility of hosting QSHE.

Magnetization in GR - HG heterostructures

Magnetization in graphene and related materials has been typically studied by adding adatom it which can be done using scanning tunneling microscopy method in a controlled manner.[42,43] Magnetization may be induced by creating vacancies or distortions in graphene.[44] However, such modulation may significantly affect the Dirac cone making graphene lose its QSHI states. Such limitations may be overcome with the proposed HG-graphene system by introducing distortions in the HG layer or by forming nanoribbons. As we shall see below, by both methods, the graphene edge states are observed in addition to significantly induced magnetic moments in the heterostructure.

First, we discuss the results of magnetization in nanoribbons. For this purpose, we constructed nanoribbons with widths up to 20 unit cells by the procedure discussed in section , in the zigzag and arm-chair conformations of the A0 and A60 systems and performed DFT calculations. The systems are further named as R0 and R60 for nanoribbons of system A0 and A60 respectively, to distinguish them from their parent systems.

We also added a prefix "Z" to denote the zigzag nanoribbon and "A" to denote the arm-chair nanoribbon. For example, a zigzag nanoribbon of A0 is denoted as ZR0, while an arm-chair nanoribbon of A60 is denoted as AR60. See table 2 for detailed nomenclature.

Table 2: Labeling schemes for all the nanoribbons.

	System A0	System A60
Arm - Chair	AR0	AR60
Zig - Zag	ZR0	ZR60

Before we discuss the electronic structure, we make note the following characteristics of the nanoribbons: (1) the structures have a unique atomic arrangement, *i.e*, even if zigzag nanoribbons are created, one of the edges is in an arm-chair configuration (see figure 8 (c)), (2) to observe the distinction between the electronics states of zigzag and arm-chair nanoribbons, their dimensions should be as large as possible.[27] The 20 unit cells width nanoribbon was the largest system that we could compute without reducing the accuracy of the cal-

culations. For each the systems, three sets of distinct DFT calculations were performed. The first set of calculations were performed on systems without any modification where the nanoribbons were constructed using the parameters described in section . In the second set of calculations, two unit cells from the center of the top HG layer were removed to introduce a defect to increase the number of edges of the HG (see figure 8 (a)). The third set of calculations were performed after saturating all the dangling bonds with hydrogen for both the systems described above. Finally, band structures for all the above systems were computed.

The band structure of the system ZR0 is given in figure 6(a). As anticipated due to the metallic nature of the systems, there is the presence of metallic states at edges. The number of edge states is even. However, the edge states are due to contributions from both conduction and valence bands. For topologically protected states, there should be a pair of bands that connects the conduction and valence bands while creating an odd number of Dirac crossing/points.[41,45] Thus, one can conclude that these states are not topologically protected. Interestingly, a presence of absolute magnetization of about 7.18 μ_B/cell is observed, causing a considerable spin split in the electronic structure of the system. This is marked in figure 6 by black arrows. This marked band originates from the edges of both HG and encapsulated GR layer. Such behavior is seen in the band structures of all of the systems (AR0, ZR60, and AR60, see figure 6) which are not hydrogenated, asserting the importance of passivation of the dangling bonds. The most remarkable observation is that the electronic structure of the systems is independent of the direction of the construction of nanoribbon or the stacking angles between the layers, $i.e$ the nanoribbons A0 (A60) and R0 (R60) have similar band structures even after selecting 20 unit cells.
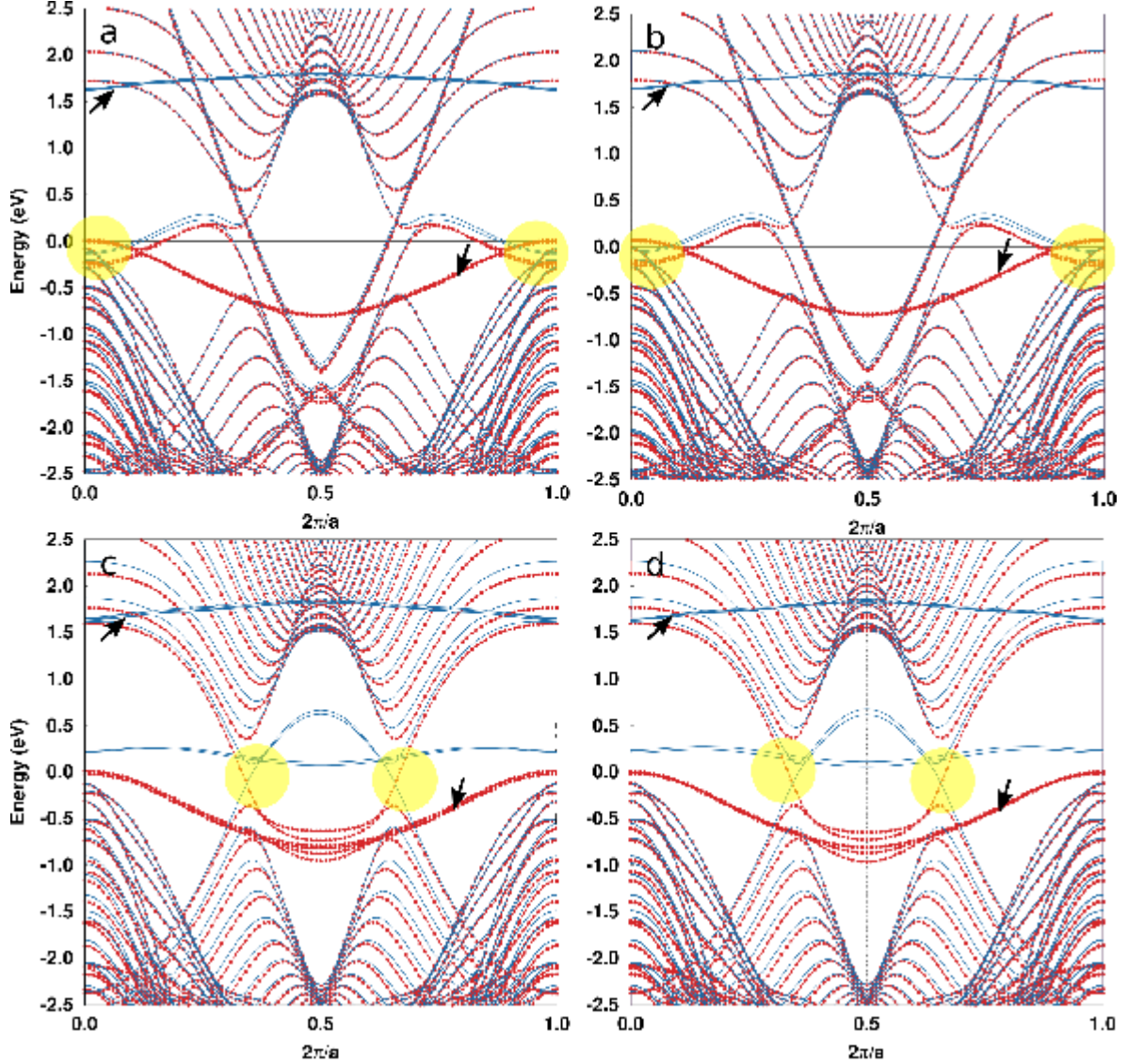
Figure 6: (color online) Band structure of (a) ZR0, (b) AR0, (c) ZR60, and (d) AR60. The red lines represent up electron bands and blue lines represent down electron bands. Some of the important features of the band structure are highlighted by yellow circles. The black arrows mark the edge states emerging from the edges of the HG layer.

We see features characteristic to the 0°and 60°stacking angle is present such as in the band structure of the ZR0 system (figure 7(a)), in the sense that the band crossing occurs at integer value of the k-point while for ZR60 system (figure 7(c)) the band crossing is observed near the half-integer k-points. This has been marked by the translucent yellow circle in figure 7. The majority of these features arise from the dangling edge bonds which have a very poor experimental realization. Upon hydrogenation, all the ribbons display a significant change

in the band structure as well as magnetization. In figure 7(b) and 7(e), we show the band structures of the passivated ZR0 and ZR60, respectively. A substantial change is observed. The absolute magnetization for both the systems is reduced drastically to about 0.47 (0.71) and 0.56 (0.69), respectively, due to saturation of the dangling bonds which is reflected well in the reduced spin splitting as compared to that of the non-hydrogenated systems. The interference from HG layers is reduced so significantly that the electronic states near the Fermi level are from the graphene sheet only.
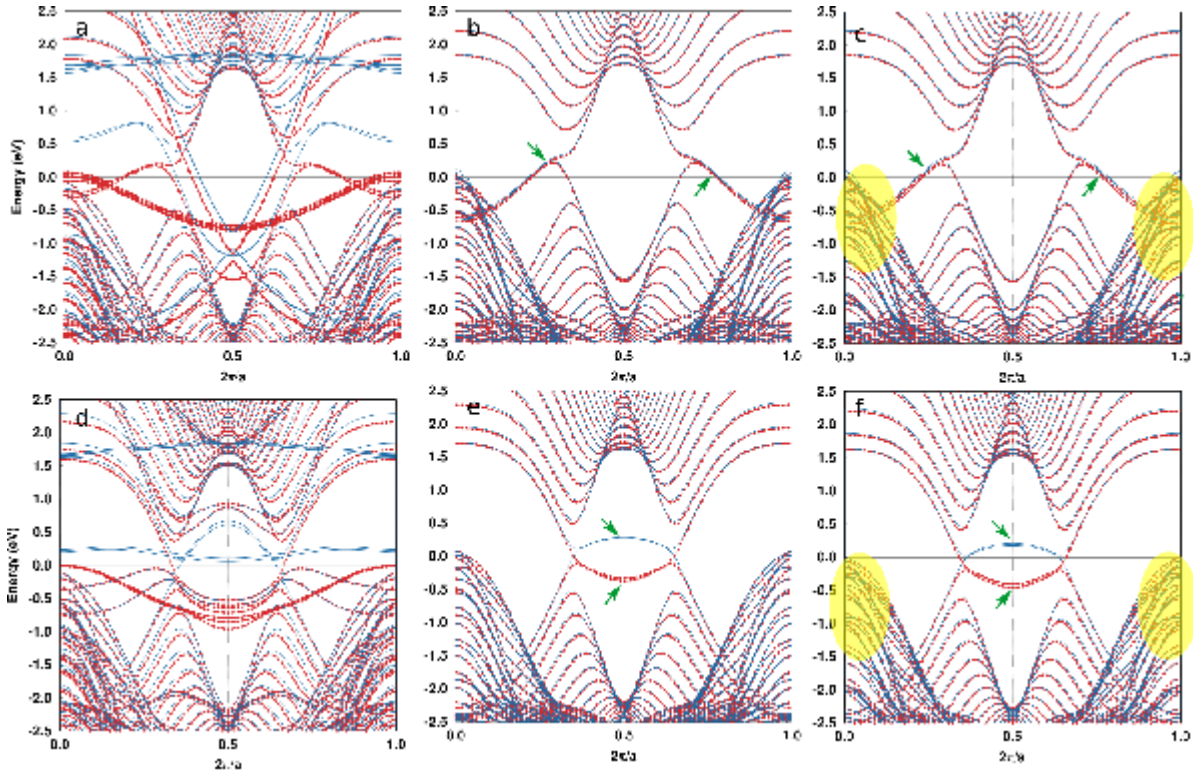

Figure 7: (color online) Band structures of (a) diss-ZR0, (b) hydrogenated ZR0, (c) hydrogenated dis-ZR0, (d) ZR60, (e) hydrogenated ZR60 and (f) hydrogenated dis-ZR60. The red lines represent up electron bands and blue lines represent down electron bands. The green arrows point to the edges states emerging from the edge atoms of graphene alone. The splitting of bands due to passivation of the HG edges have been marked by yellow ovals.

It is only logical from this discussion that further calculations can be carried out either on zigzag or armchair ribbons. We carried out the calculations on zigzag ribbons: ZR0 and ZR60. Further, in order to modulate magnetization, we introduce distortions in these systems by removing two unit cells from one of the HG layers. We label these distorted nanoribbons

as "diss-ZR0 (diss-ZR60)", respectively. In figure 7(a) and 7(c), we show the band structures of the diss-ZR0 (non-hydrogenated and passivated), 7(d) and 7(f) band structures for diss-ZR60 (non-hydrogenated and passivated), respectively. Due to the presence of an additional HG edge, an increase in the absolute magnetization is observed. It has now increased to 7.49 μ_B/cell for diss-ZR0 further increasing the split in the band structure. As mentioned earlier the major contribution to this split is from the edges of the HG. However, for diss-ZR60, the magnetization has decreased by a small value to 7.14 μ_B/cell. This also explains the decrease in the number of degenerate bands. Thus, by just increasing the number of edges of HG, the magnetization of the proposed system can be altered: an additional parameter for customization of the proposed system.

Interestingly, after hydrogenation, the band structures of distorted ribbons seem to resemble those of the undistorted ribbons (compare figure 7(b) for band structure of ZR0 with that of diss-ZR0, in figure 7(c)). However, this observation seems to be misleading as on closer analyzes we found that there are some noticeable and important differences. Firstly, there is a small increase in the spin-split due to increase in edges. These spin-split states are primarily in the vicinity of the k=0 and $2\pi/a$, marked by yellow translucent ovals. This may imply that by fine-tuning the number of edges of HG, one can increase the magnetization of the ribbon without significantly interfering the GR states at the Fermi level. However, in order to retain most of the features of the graphene states, especially the Dirac cone, one may have to increase the width of the nanoribbon up to 50 units cells or more.[27]
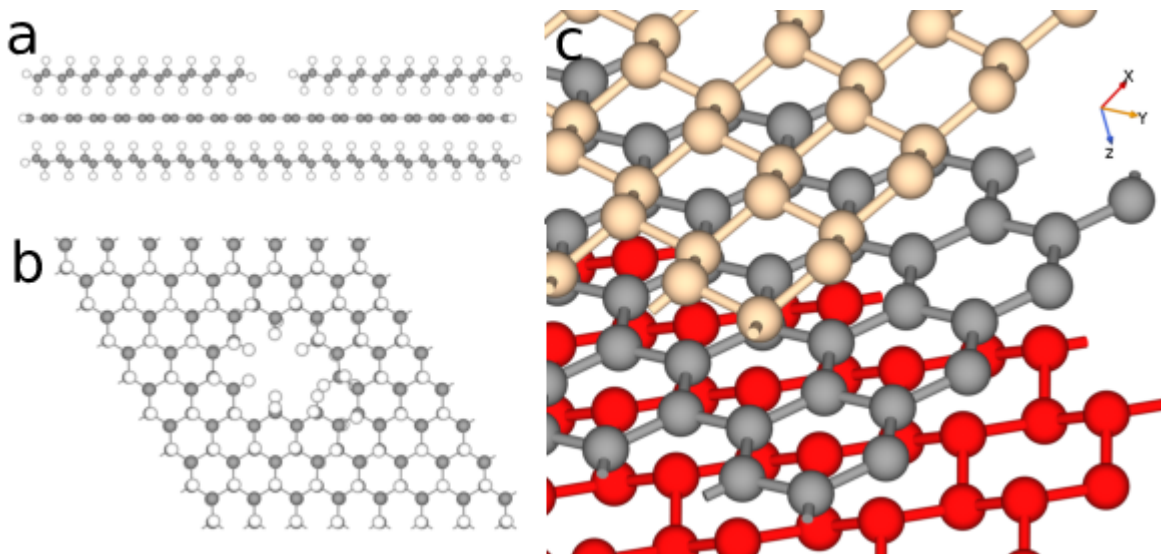
Figure 8: (color online) (a) Side view of the nanoribbon with two unit cells removed form the top HG layer, (b) top view of the top HG layer of the system A0 showing the cavity, (c) the edges of the system AR60. The hydrogen atoms of the system have been removed. The top HG is represented by pinkish/brownish color while the bottom HG is represented using red color. The graphene layer is colored in grey. Note that the edge of graphene layer is armchair whereas that of HG are zigzag.

Adsorption of Molecules on GR-HG heterostructures

Graphene with substitutional non-metal dopants or adatoms has been widely studied for applications in sensing molecules and electrocatalysis.[46] In this section, we test the applicability of the proposed system for adsorption of molecules such as H_2, O_2, carbon dioxide, and ethanol. As it has been proposed that QSHI like stanene can also be utilized for gas sensing applications,[47] a brief investigation was performed on the proposed system. Concluded from the above, either by non-passivation of the edges or by increasing the distortions in one of the HG layers, magnetization can fine tune. The magnetization in these systems can certainly be affected by the presence of additional factors like adsorbed molecules. For this purpose, a base system consisting of 8×8×1 number of unit cells of the system A0 was created. In order to induce magnetization, an asymmetric cavity was created on the top HG which was hydrogenated, since such a vacancy or impurities is required as these molecules generally do not get adsorbed on defect-free surfaces. In figure 9, we show the image of the top HG

with the cavity along with the optimized structure of adsorbed H_2, O_2, CO_2 and ethanol molecules on the system A0. The adsorbed H_2 molecule is shown in the yellow translucent circle in figure 9a.
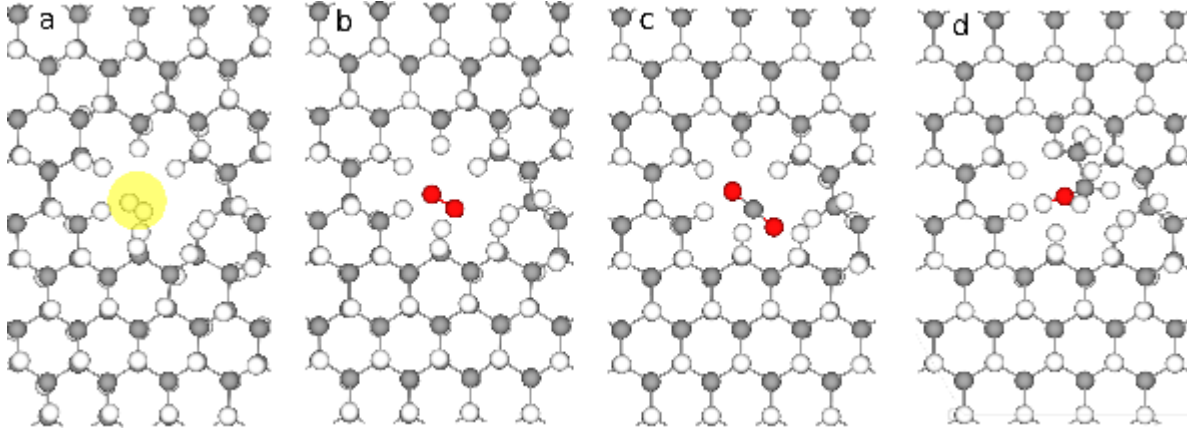

Figure 9: (color online) Structure of molecules adsorbed on HG-graphene-HG trilayer system with cavity in the top HG layer. Only the top HG layer is shown. (a) H_2 molecule (in yellow region), (b) O_2 molecule, (c) CO_2 molecule and (d) ethanol molecule.

Table 3: Magnetization induced due to the presence of cavity and upon adsorption of molecules on to the system A0.

Name	Absolute Magnetization ($\mu_B/cell$)
System A0	0.1
A0 : H_2	2.35
A0 : O_2	7.23
A0 : CO_2	7.28
A0 : ethanol	7.29

Geometry optimization of the distorted A0 system with the molecules adsorbed was carried out. These molecules are likely to change the magnetization upon adsorption on the A0 surface. However, the total number of the atoms exceeds 600 making the geometry optimization within DFT framework difficult. Hence, we performed the geometry optimization using the Brenner force field for the substrate distorted A0 system and RelaxFF force field for the adsorbed molecules as implemented in ATK VNL package[35] until the maximum absolute forces on the atoms were less than 10^{-4} eV/Å. Then the optimized geometry was used to

calculate magnetization using DFT. The DFT parameters are kept the same as described in section , except that the calculations were performed for Γ-point only due to a large number of atoms. We observed a distinct and significant change in the magnetization of the system for each molecule as summarized in Table 3. These changes can be easily detected in the experiments. Hence, we may conclude that the proposed system can be used to detect these molecules.

Conclusion

We performed DFT calculations on hydrogenated graphene - graphene trilayer systems with PBE exchange-correlation potential including the DFT-D2 Van der Waals correction for representing accurately the phonon dispersion effects. We found that the heterostructure of graphene encapsulated by hydrogenated graphene could be a promising candidate for a variety of device applications. A detailed investigation shows that this system does have a possibility of preserving and protecting the edge states of GR. The presence of the HG layer makes the system magnetic which can further be tuned by controlling the vacancies in HG layers. These defects or vacancies in the outermost HG layer can also be used to detect molecules such as H_2, O_2, CO_2 and ethanol since upon adsorption a significant change in magnetic moments is observed which can be detected experimentally. An additional important feature that was noted was the system independence on the direction of nanoribbons providing an additional simplicity for experimental realization of the proposed system. Our results on trilayer graphene encapsulated by HG indicate that the above observations can be extended to these systems with a larger number of central graphene layers. Interestingly, such systems are relatively simpler to fabricate by first exfoliating or synthesizing multilayer graphene and then hydrogenating the outermost layers. This work brings out the versatility of the multilayer GR sandwiched between two HG layers and thus has the merit of being experimentally investigated.

Acknowledgement

Supporting Information Available

The following files are available free of charge. See supplementary information for the crystal structure data, band structures of HG encapsulated bilayer and trilayer graphene, k-resolved projected density of states (PDOS) and charge densities.

- Section I : Coordinates of Proposed Systems

- Section II : Band structure of Trilayer graphene encapsulated with HG

- Section III : k-resolved Projected Density of States

- Section IV : Charge Density

- Section V : Selected k-resolved PDOS of nanoribbon

- Section VI : Bilayer Structures

- Section VII : Band structure of unstable system

References

(1) Haldane, F. D. M. Model for a quantum Hall effect without Landau levels: Condensed-matter realization of the" parity anomaly". *Phys. Rev. Lett.* **1988**, *61*, 2015

(2) Kane, C. L.; Mele, E. J. Quantum spin Hall effect in graphene. *Phys. Rev. Lett.* **2005**, *95*, 226801

(3) König, M.; Wiedmann, S.; Brüne, C.; Roth, A.; Buhmann, H.; Molenkamp, L. W.; Qi, X.-L.; Zhang, S.-C. Quantum spin Hall insulator state in HgTe quantum wells. *Science* **2007**, *318*, 766–770

(4) Ren, Y.; Qiao, Z.; Niu, Q. Topological phases in two-dimensional materials: a review. *Reports on Progress in Physics* **2016**, *79*, 066501

(5) Zhu, F.-f.; Chen, W.-j.; Xu, Y.; Gao, C.-l.; Guan, D.-d.; Liu, C.-h.; Qian, D.; Zhang, S.-C.; Jia, J.-f. Epitaxial growth of two-dimensional stanene. *Nature materials* **2015**, *14*, 1020–1025

(6) Deng, J.; Xia, B.; Ma, X.; Chen, H.; Shan, H.; Zhai, X.; Li, B.; Zhao, A.; Xu, Y.; Duan, W. , et al. Epitaxial growth of ultraflat stanene with topological band inversion. *Nature materials* **2018**, *17*, 1081

(7) Saxena, S.; Chaudhary, R. P.; Shukla, S. Stanene: atomically thick free-standing layer of 2D hexagonal tin. *Scientific reports* **2016**, *6*, 31073

(8) Ghadiyali, M.; Chacko, S. Band splitting in bilayer stanene electronic structure scrutinized via first principle DFT calculations. *https://doi.org/10.1016/j.cocom.2018.e00341* **2018**,

(9) Wakamura, T.; Reale, F.; Palczynski, P.; Guéron, S.; Mattevi, C.; Bouchiat, H. Strong Anisotropic Spin-Orbit Interaction Induced in Graphene by Monolayer WS 2. *Physical review letters* **2018**, *120*, 106802

(10) Rickhaus, P.; Wallbank, J.; Slizovskiy, S.; Pisoni, R.; Overweg, H.; Lee, Y.; Eich, M.; Liu, M.-H.; Watanabe, K.; Taniguchi, T. , et al. Transport through a network of topological channels in twisted bilayer graphene. *Nano letters* **2018**, *18*, 6725–6730

(11) Fan, Y.; Zhao, M.; Wang, Z.; Zhang, X.; Zhang, H. Tunable electronic structures of graphene/boron nitride heterobilayers. *Applied Physics Letters* **2011**, *98*, 083103

(12) Avsar, A.; Tan, J. Y.; Taychatanapat, T.; Balakrishnan, J.; Koon, G.; Yeo, Y.; Lahiri, J.; Carvalho, A.; Rodin, A.; O?Farrell, E. , et al. Spin–orbit proximity effect in graphene. *Nature communications* **2014**, *5*, 4875

(13) Gmitra, M.; Fabian, J. Graphene on transition-metal dichalcogenides: A platform for proximity spin-orbit physics and optospintronics. *Physical Review B* **2015**, *92*, 155403

(14) Wang, Z.; Tang, C.; Sachs, R.; Barlas, Y.; Shi, J. Proximity-induced ferromagnetism in graphene revealed by the anomalous Hall effect. *Physical review letters* **2015**, *114*, 016603

(15) Mendes, J.; Santos, O. A.; Meireles, L.; Lacerda, R.; Vilela-Leão, L.; Machado, F.; Rodríguez-Suárez, R.; Azevedo, A.; Rezende, S. Spin-current to charge-current conversion and magnetoresistance in a hybrid structure of graphene and yttrium iron garnet. *Physical review letters* **2015**, *115*, 226601

(16) Wei, P.; Lee, S.; Lemaitre, F.; Pinel, L.; Cutaia, D.; Cha, W.; Katmis, F.; Zhu, Y.; Heiman, D.; Hone, J. , et al. Strong interfacial exchange field in the graphene/EuS heterostructure. *Nature materials* **2016**, *15*, 711

(17) Sata, Y.; Moriya, R.; Morikawa, S.; Yabuki, N.; Masubuchi, S.; Machida, T. Electric field modulation of Schottky barrier height in graphene/MoSe2 van der Waals heterointerface. *Applied Physics Letters* **2015**, *107*, 023109

(18) Neek-Amal, M.; Peeters, F. Graphene on boron-nitride: Moiré pattern in the van der Waals energy. *Applied Physics Letters* **2014**, *104*, 041909

(19) Dean, C. R.; Young, A. F.; Meric, I.; Lee, C.; Wang, L.; Sorgenfrei, S.; Watanabe, K.;

Taniguchi, T.; Kim, P.; Shepard, K. L. , et al. Boron nitride substrates for high-quality graphene electronics. *Nature nanotechnology* **2010**, *5*, 722

(20) Song, X.; Sun, J.; Qi, Y.; Gao, T.; Zhang, Y.; Liu, Z. Graphene/h-BN Heterostructures: Recent Advances in Controllable Preparation and Functional Applications. *Advanced Energy Materials* **2016**, *6*

(21) Yang, W.; Chen, G.; Shi, Z.; Liu, C.-C.; Zhang, L.; Xie, G.; Cheng, M.; Wang, D.; Yang, R.; Shi, D. , et al. Epitaxial growth of single-domain graphene on hexagonal boron nitride. *Nature materials* **2013**, *12*, 792

(22) Davies, A.; Albar, J. D.; Summerfield, A.; Thomas, J. C.; Cheng, T. S.; Korolkov, V. V.; Stapleton, E.; Wrigley, J.; Goodey, N. L.; Mellor, C. J. , et al. Lattice-matched epitaxial graphene grown on boron nitride. *Nano letters* **2017**, *18*, 498–504

(23) San-Jose, P.; Gutiérrez-Rubio, A.; Sturla, M.; Guinea, F. Spontaneous strains and gap in graphene on boron nitride. *Physical Review B* **2014**, *90*, 075428

(24) Lin, Y.-C.; Ghosh, R. K.; Addou, R.; Lu, N.; Eichfeld, S. M.; Zhu, H.; Li, M.-Y.; Peng, X.; Kim, M. J.; Li, L.-J. , et al. Atomically thin resonant tunnel diodes built from synthetic van der Waals heterostructures. *Nature communications* **2015**, *6*, 7311

(25) Shi, Y.; Zakharov, A. A.; Ivanov, I. G.; Yazdi, G. R.; Jokubavicius, V.; Syväjärvi, M.; Yakimova, R.; Sun, J. Elimination of step bunching in the growth of large-area monolayer and multilayer graphene on off-axis 3CSiC (111). *Carbon* **2018**, *140*, 533–542

(26) Tada, K.; Haruyama, J.; Yang, H.; Chshiev, M.; Matsui, T.; Fukuyama, H. Ferromagnetism in hydrogenated graphene nanopore arrays. *Physical review letters* **2011**, *107*, 217203

(27) Neto, A. C.; Guinea, F.; Peres, N. M.; Novoselov, K. S.; Geim, A. K. The electronic properties of graphene. *Reviews of modern physics* **2009**, *81*, 109

(28) Giannozzi, P.; Baroni, S.; Bonini, N.; Calandra, M.; Car, R.; Cavazzoni, C.; Ceresoli, D.; Chiarotti, G. L.; Cococcioni, M.; Dabo, I. , et al. QUANTUM ESPRESSO: a modular and open-source software project for quantum simulations of materials. *J. of Phys. Cond. Matt.* **2009**, *21*, 395502

(29) Perdew, J. P.; Burke, K.; Ernzerhof, M. Generalized Gradient Approximation Made Simple. *Phys. Rev. Lett.* **1996**, *77*, 3865–3868

(30) Barone, V.; Casarin, M.; Forrer, D.; Pavone, M.; Sambi, M.; Vittadini, A. Role and effective treatment of dispersive forces in materials: Polyethylene and graphite crystals as test cases. *Journal of Computational Chemistry* **2009**, *30*, 934–939

(31) Grimme, S. Semiempirical GGA-type density functional constructed with a long-range dispersion correction. *Journal of Computational Chemistry* **2006**, *27*, 1787–1799

(32) PS Library version 1.0 Pseudopotentials. `https://dalcorso.github.io/pslibrary/`

(33) Dal Corso, A. Pseudopotentials periodic table: From H to Pu. *Computational Materials Science* **2014**, *95*, 337–350

(34) Kokalj, A. Computer graphics and graphical user interfaces as tools in simulations of matter at the atomic scale. *Comp. Mat. Sci.* **2003**, *28*, 155–168

(35) Virtual NanoLab version 2017.0, QuantumWise A/S. `www.quantumwise.com`

(36) Fan, X.; Zheng, W.; Kuo, J.-L.; Singh, D. J.; Sun, C.; Zhu, W. Modulation of electronic properties from stacking orders and spin-orbit coupling for 3R-type MoS2. *Sci. Rep.* **2016**, *6*, 24140

(37) Generally, presence of negative frequencies indicate a structural instability. However, in this case, a careful examination of the phonon frequencies is required before coming to a conclusion. The magnitude of negative phonon frequencies is not significant and so is it's spread in momentum space, *i.e.* they are localized near the Γ-point only, for

most of the systems. We have increased various input parameters such as the cutoff radius, number of k-points for optimization, and found it to reduce the range of k-points with negative frequencies. Thus, these small magnitude and spread of negative frequencies are likely due to numerical instabilities or errors rather than the structural instability. In addition, we also observed that the change in the electronic properties are negligible when compaired with the structure having a higher negative phonon dispersion. Further: these negative frequencies are between two successive special k-points within the Brillouin zone, which generally raises due to out-of plane buckling and/or due to the strain due to lattice mismatch, as explain in text. Here these negative frequencies are very weak comparison, hence upon fabrication on a substrate they are likely to die out.

(38) Mounet, N.; Gibertini, M.; Schwaller, P.; Campi, D.; Merkys, A.; Marrazzo, A.; Sohier, T.; Castelli, I. E.; Cepellotti, A.; Pizzi, G. , et al. Two-dimensional materials from high-throughput computational exfoliation of experimentally known compounds. *Nature nanotechnology* **2018**, *13*, 246

(39) Datta, B.; Dey, S.; Samanta, A.; Agarwal, H.; Borah, A.; Watanabe, K.; Taniguchi, T.; Sensarma, R.; Deshmukh, M. M. Strong electronic interaction and multiple quantum Hall ferromagnetic phases in trilayer graphene. *Nature communications* **2017**, *8*, 14518

(40) Soluyanov, A. A.; Vanderbilt, D. Computing topological invariants without inversion symmetry. *Physical Review B* **2011**, *83*, 235401

(41) Bansil, A.; Lin, H.; Das, T. Colloquium: Topological band theory. *Reviews of Modern Physics* **2016**, *88*, 021004

(42) Eigler, D. M.; Schweizer, E. K. Positioning single atoms with a scanning tunnelling microscope. *Nature* **1990**, *344*, 524

(43) Nafday, D.; Saha-Dasgupta, T. Magnetism of an adatom on bilayer graphene and its control: A first-principles perspective. *Physical Review B* **2013**, *88*, 205422

(44) Palacios, J. J.; Fernández-Rossier, J.; Brey, L. Vacancy-induced magnetism in graphene and graphene ribbons. *Physical Review B* **2008**, *77*, 195428

(45) Hasan, M. Z.; Kane, C. L. Colloquium: topological insulators. *Reviews of modern physics* **2010**, *82*, 3045

(46) Fazio, G.; Ferrighi, L.; Perilli, D.; Di Valentin, C. Computational electrochemistry of doped graphene as electrocatalytic material in fuel cells. *International Journal of Quantum Chemistry* **2016**, *116*, 1623–1640

(47) Takahashi, L.; Takahashi, K. Low temperature pollutant trapping and dissociation over two-dimensional tin. *Phys. Chem. Chem. Phys.* **2015**, *17*, 21394–21396